MASARYKOVA UNIVERZITA
PŘÍRODOVĚDECKÁ FAKULTA
ÚSTAV TEORETICKÉ FYZIKY A ASTROFYZIKY

Bakalářská práce

BRNO 2019   TOMÁŠ PLŠEK

MASARYKOVA UNIVERZITA

UNIVERZITA

PŘÍRODOVĚDECKÁ FAKULTA
ÚSTAV TEORETICKÉ FYZIKY A ASTROFYZIKY

Modelování temné hmoty v kupách galaxií

Bakalářská práce

Tomáš Plšek

Vedoucí práce: Mgr. Filip Hroch Ph.D.   Brno 2019

Bibliografický záznam

Bibliographic Entry

Abstrakt

Neznámá materie, označovaná jako temná hmota, by podle současných kosmologických modelů měla tvořit valnou část veškeré hmoty ve vesmíru. Tento druh hmoty však nejsme schopni přímo pozorovat, neboť se předpokládá, že nepodléhá elektromagnetické interakci, a tedy nemůže ani zářit. Případný výskyt temné hmoty je možné odhalit pouze u velkoškálových objektů jako jsou galaxie a galaktické kupy, a to pouze nepřímo pomocí gravitačního působení na hmotu svítivou. V této bakalářské práci se věnujeme vytváření počítačových modelů hal temné hmoty právě kolem galaktických kup. Tyto modely porovnáváme s reálnými měřeními svítivé hmoty v kupách galaxií.

Abstract

According to the current cosmological model, unknown kind of matter called dark matter should form most of all the matter in the Universe. However, we are unable to directly observe this kind of matter because it is expected that it is not subject to electromagnetic interaction, and therefore cannot emit light. An eventual occurrence of dark matter can be revealed only in large-scale objects such as galaxies and galaxy clusters, and only indirectly due to their gravitational interaction with visible matter. In this thesis, we create computer models of dark matter halo's around galaxy clusters and compare those models to real measurements of visible matter in galaxy clusters.

MASARYKOVA UNIVERZITA
Přírodovědecká fakulta

ZADÁNÍ BAKALÁŘSKÉ PRÁCE

Akademický rok: 2018/2019

Ústav: Ústav teoretické fyziky a astrofyziky

Student: Tomáš Plšek

Program: Fyzika

Obor: Astrofyzika

Ředitel *Ústavu teoretické fyziky a astrofyziky* PřF MU Vám ve smyslu Studijního a zkušebního řádu MU určuje bakalářskou práci s názvem:

Název práce: Modelování temné hmoty v kupách galaxií

Název práce anglicky: Dark matter modelling of galaxy clusters

Oficiální zadání:
Přestože je Vesmír z podstatné části složen, z temné hmoty a energie, o jejichž skutečné podstatě je známo jen velmi málo, věříme, že s pomocí běžně pozorované svítivé hmoty se nám podaří ji zkoumat.

Klíčem k jejímu poznání by snad mohly být obecné matematické modely a pozorování objektů jejichž gravitační pole je dáno především temnou hmotou: jde především o kosmologické simulace a galaktické kupy pozorované v rentgenovém oboru.

Cílem práce by mělo být modelování hal z temné hmoty kolem galaktických kup. Tyto modely mohou objasnit vnitřní strukturu těchto objektů, jejich formování či interakce mezi galaxiemi. Samotné kupy galaxií umožňují, díky horkému plynu, porovnat výsledky simulací s reálnými daty.

Ke získání relevantních výsledků bude třeba využít nejnovějších poznatků matematických, fyzikálních a počítačových metod.

Jazyk závěrečné práce: angličtina

Vedoucí práce: Mgr. Filip Hroch, Ph.D.

Datum zadání práce: 7. 12. 2018

V Brně dne: 28. 1. 2019

Souhlasím se zadáním (podpis, datum):

. . . .
Tomáš Plšek
student

. . . .
Mgr. Filip Hroch, Ph.D.
vedoucí práce

. . . .
prof. Rikard von Unge, Ph.D.
ředitel Ústavu teoretické fyziky a astrofyziky

Poděkování

Na tomto místě bych chtěl poděkovat svému vedoucímu doktoru Filipu Hrochovi za píli a výdrž při konzultacích a za cené rady při psaní této bakalářské práce.

Prohlášení

Prohlašuji, že jsem svoji bakalářskou práci vypracoval samostatně s využitím informačních zdrojů, které jsou v práci citovány.

Brno 22. května 2019

. . . .
Tomáš Plšek

Contents

Introduction

The observable part of the Universe is made out of known atomic and subatomic particles. These particles may form objects like planets, asteroids, stars and hot or cold gas clouds. Solar systems or other hierarchical structures are composed of these planets, stars and clouds. When there is a lot of stars, they may group into star clusters – open clusters or globular clusters. Galaxies consist of star clusters, single stars, nebulas, gas clouds and galactic halos and merge into galaxy clusters. Galaxy clusters group into superclusters and superclusters form filaments and so-called walls which seem to be the biggest structures in the Universe. On bigger scales, the Universe resembles a foam – it is made out of these walls and voids which are technically only vast empty spaces. On such scales, the Universe seems to be homogeneous (same at every point – translational symmetry) and isotropic (same in every direction – rotational symmetry) although the homogeneity and isotropy are not exact and some perturbation (density fluctuations) occures.

In the Universe, there are three fundamental interactions: strong nuclear force, electroweak force and gravity. Most of the objects mentioned in the previous paragraph are mainly subject to the gravitational force. Their formation and dynamics depend on how much matter the object has or how big it is. The larger the objects are the more applies at first the dark matter (galaxies, galaxy clusters) a then also the dark energy (galaxy clusters, superclusters). Dark matter (DM) is a hypothetical form of matter that interacts with classical matter only gravitationally. It could probably also weakly interact with itself (self-interacting dark matter SIDM). It was implemented due to discrepancy of the velocity profile of visible matter in galaxies. In general, if the galaxies would consist only of visible matter, they could not rotate at such velocities. If there was not some extra matter in the form of DM, the galaxies would fall apart. The dark energy (DE) plays a similar role as dark matter. It was introduced to describe the accelerating expansion of the Universe – for distant objects we observe considerable redshift which signifies they are moving away from us at high speeds. On large scales, dark energy defeats the gravitational pull of matter (baryonic matter and DM) which means there is a limit for objects to be gravitationally bound – the biggest objects held together by their own gravity are the galaxy clusters. Galaxy clusters and their evolution and dynamics are therefore the best topics for further exploration and opportune confirmation of both dark matter and dark energy existence.

In a galaxy cluster, we can directly observe only visible classical matter (stars, hot gas clouds or other light sources). But the visible matter is just a part of the total amount of baryonic matter ($6 - 24\,\%$; Laganá et al. 2008) which is only a fraction of all matter ($7 - 15\,\%$; Laganá et al. 2008) in the cluster. The rest of the material particles are supposed to be in the form of dark matter. If we would convert all the matter to the energy it would still make only less than about a third of the total energy in the cluster. The remaining two-thirds belong to dark energy. It is clear that the evolution of a galaxy cluster is mainly managed by dark matter and dark energy. Unfortunately, we are currently not able to directly observe neither of them.

To understand the evolution of the Universe or a galaxy cluster, we need to make a general cosmological model and then compare the model to real data. The model can be verified by making a

computer numerical simulation, with corresponding parameters, that will compute the evolution of a chosen system. Then we can compare for instance density or temperature profiles of such systems to real measurements of clusters (the measuring methods and measurable quantities are listed in Chapter 2). Presently, the widely accepted model is the Lambda Cold Dark Matter (ΛCDM) model which is in detail described in Chapter 1. This model, as its name suggests, applies both dark matter and dark energy. The Λ stands for cosmological constant from Einstein's field equations. In his equations it was introduced to keep the Universe static; in the ΛCDM model it has quite the opposite meaning.

Nowadays, thanks to highly developed computer technology and also very good algorithms, we are able to make really good simulations that are in very strong agreement with observed data. There is plenty of codes for N-body cosmological simulations that use the ΛCDM model. In this thesis, we use code *Gadget-2* by Springel (2005*a*), further described in Chapter 3. The code uses approximative techniques to reduce the computational time and Peano-Hilbert curve and domain decomposing techniques to make the code executable using multiple CPU's.

1. Cosmological Model

There are several models, that try to describe the Universe on the cosmological scale and provide quite good predictions about its early phases. They mostly expect that our Universe began with a "Big Bang" and then rapidly ($10^{-36} - 10^{-32}$ s) inflated[1] into huge size. It was enormously dense and hot at this period of time. After the inflationary epoch, when all four interactions separated (at about 10^{-12} s), the baryogenesis started and the Universe was filled with quark-gluon plasma. Classical hadrons (protons, antiprotons, neutrons, antineutrons) came to exist when the Universe was only about a microsecond old. At the end of this hadron era, most of hadrons and anti-hadrons annihilated[2]. The hadron era is followed by the lepton era. Such Universe was still pretty hot and dense. It was filled with protons, electrons and also photons, but due to its high density and temperature, photons were scattered on free electrons and the Universe was opaque. (edited from Zejda 2017)

At about 400 thousand years after the Big Bang, the "last" free electrons recombined on protons, photons were no more scattered on free electrons and the Universe has become transparent. This is the era when the Cosmic Microwave Background (CMB) came to exist. As the temperature map of CMB (fig 1.1) shows, the matter was distributed almost homogeneously and isotropically with relatively small fluctuations. The CMB has spectrum very similar to spectrum of a black-body at temperature 2.72548 ± 0.00057 K (Fixsen 2009). The period of time between the emergence of CMB and formation of first stars is called "dark ages", because there was no source of light at this time. During the dark ages, the formation of galaxy clusters and galaxies began and this is the phase of the Universe when dark matter and dark energy came to the scene.

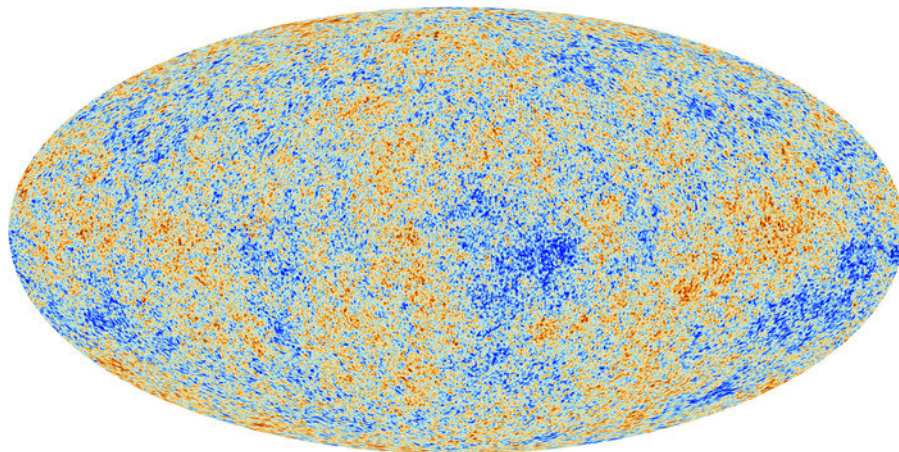Figure 1.1: Temperature map of Cosmic Microwave Background obtained by Planck (ESA 2013).

---

[1]It was the space itself, what inflated. The Universe can not expand anywhere, because it contains all the space.

[2]The fact, that we now live in the universe made solely of matter and not antimatter, is now one of the biggest problems of the ΛCDM model. Inflationary phase of the Universe could be an explanation.

1.1 ΛCDM cosmology

Currently, the widely accepted cosmological model is the Lambda Cold Dark Matter (ΛCDM) model. As said in the introduction both dark matter and dark energy, as well as primordial fluctuations, play a crucial role in ΛCDM cosmology. Dark matter and dark energy determine the evolution of the system and primordial fluctuations can be imagined as a set of initial conditions (density, temperature and velocity distributions). The effect of dark components can be described by Friedmann equations (Friedman's solutions to Einstein's field equations).

The position of a point in space is classically being described by its physical coordinates **r**. In a homogeneous expanding space, we can implement a scale factor $a(t)$ which is the dimensionless time-dependent quantity and describes the expansion of space. At present-day Universe the value of scale factor is $a(t_0) = 1$. Applying that, we can change to the different coordinate system: so-called comoving coordinates **x**. The relationship between physical and comoving coordinates is expressed by the scale factor

$$\mathbf{r} = a(t)\,\mathbf{x}. \tag{1.1}$$

The scale factor causes that, although the physical coordinates of an object in an expanding Universe do change, comoving coordinates do not (as Figure 1.2 illustrates).

The expansion can be also described from the view of the observer and that by the Hubble's law which describes how fast are distant objects moving away from us. The radial velocity of an object is due to expansion of space directly proportional to its distance and the proportionality factor is the Hubble parameter

$$\mathbf{v} = H\,\mathbf{r}. \tag{1.2}$$

For the Hubble parameter it is expected, that it actually varied in time. Using (1.1) and (1.2) we can express the Hubble parameter as a function of the scale factor

$$H(t) = \frac{\dot{\mathbf{r}}}{\mathbf{r}} = \frac{\dot{a}(t)}{a(t)}. \tag{1.3}$$

Hubble parameter is often mistakenly called Hubble constant. Hubble constant is the value we measure today and the measurements move around $70\ \mathrm{km\,s^{-1}\,Mpc^{-1}}$.

The exact value of the Hubble constant depends on the measuring method. For the early phases of the Universe was measured the value $H_0 = 67.78\ \mathrm{km\,s^{-1}\,Mpc^{-1}}$(for flat ΛCDM model; Ryan et al. 2019)[3]. The measurements of the relatively near objects give us slightly higher value $H_0 = 74.03 \pm 1.42\ \mathrm{km\,s^{-1}\,Mpc^{-1}}$ (Riess et al. 2019)[4]. The difference between the values is considerable (more than $6\ \mathrm{km\,s^{-1}\,Mpc^{-1}}$) and has not been explained yet.

1.1.1 Friedmann equations

The Friedmann equations were derived from the equations of general relativity, by introducing the scale factor of the Universe $a(t)$. Solutions of Friedmann equations well describe the formation and dynamics of a static or constantly expanding Universe. Friedmann equations allow us to formulate the Hubble parameter $H(t)$ as a function of total energy density ρ and space curvature k

$$H^2 = \left(\frac{\dot{a}}{a}\right)^2 = \frac{8\pi G}{3}\rho - \frac{kc^2}{a^2}, \tag{1.4}$$

---

[3]The value was obtained from measurements of Baryon Acoustic Oscillations (BAO).

[4]The value was estimated by combining measurements of the detached eclipsing binaries in the LMC and masers in NGC 4258
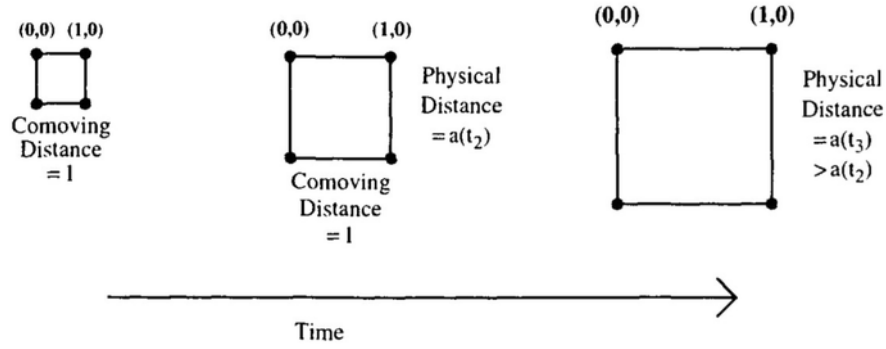
Figure 1.2: The relation between physical and comoving coordinates in homogeneously and isotropically expanding space (Pandey 2016).

where G is the gravitational constant and c is the speed of light. Density is related to scale factor and pressure via the fluid equation

$$\dot{\rho} + 3\frac{\dot{a}}{a}\left(\rho + \frac{p}{c^2}\right) = 0. \tag{1.5}$$

The speed of light is often set to $c = 1$ which makes time and space units and also matter and energy densities interchangeable: $t \sim a$, $\rho \sim \varepsilon$. The equation (1.4) is not able to describe the earliest phases of the Universe. For an accelerate expanding Universe the cosmological constant Λ must be implemented

$$H^2 = \left(\frac{\dot{a}}{a}\right)^2 = \frac{8\pi G}{3}\rho - \frac{k}{a^2} + \frac{\Lambda}{3}. \tag{1.6}$$

If we put cosmological constant equal to zero and assume that the Universe is now flat ($k = 0$), we get the relationship for the critical density

$$\rho_{\text{crit}} = \frac{3H^2}{8\pi G}. \tag{1.7}$$

The critical density does not have to be the exact value of the mean density of the Universe, but it is a good estimation. The actual value of mean density should be within an order of magnitude from the critical density. The critical density is in standard units (kilograms and meters) and in cosmological units (solar masses and megaparsecs) equal to

$$\rho_{\text{crit}} = 1.88\, h^2\, 10^{-26}\, \text{kg}\,\text{m}^{-3} = 2.78\, h^{-1}\, 10^{11}\, M_{\odot} / (h^{-1}\, \text{Mpc})^3 \tag{1.8}$$

where h is the dimensionless Hubble parameter ($h = H_0 / 100\,\text{km}\,\text{s}^{-1}\,\text{Mpc}^{-1}$). Using the critical density we can now define the density parameter $\Omega = \rho / \rho_{\text{crit}}$. The density parameter can be used for all densities: dark energy (Λ), dark matter (DM), baryonic matter (bar), radiation (rad) and space curvature (k). Using (1.4) and (1.6) we can define the curvature density parameter and the dark energy density parameter

$$\Omega_k = -\frac{k}{a^2 H^2}, \quad \Omega_\Lambda = \frac{\Lambda}{3H^2}. \tag{1.9}$$

Although the cosmological constant Λ or space curvature k might be constants, their density parameters may vary in time due to time-dependency of the Hubble parameter (equations taken from Liddle 2003).

1.1.2 Equation of state

If we define the dark energy density as $\rho_\Lambda = \Lambda/(8\pi G)$, we can rewrite (1.6) to

$$H^2 = \frac{8\pi G}{3}(\rho + \rho_\Lambda) - \frac{k}{a^2}. \tag{1.10}$$

Using (1.5) and the fact that ρ_Λ is constant we get the relationship between dark energy density and pressure $p_\Lambda = -\rho_\Lambda c^2$ which means dark energy has a negative pressure. If we assume that cosmological constant is not perfectly constant and exhibits slow linear variation and if we set $c = 1$, we get

$$p_\Lambda = w(a)\rho_\Lambda, \quad w(a) = w_0 + w_a(1-a), \tag{1.11}$$

where w represents the equation of state of a perfect fluid. This principle is called *quintessence*. Currently, the value of the equation of state seems to be really near or exactly -1 . (edited from Liddle 2003)

1.2 Geometry of the Universe

Now we can express the Hubble parameter using density parameters and get the well known equation

$$H(a) = \frac{\dot{a}}{a} = H_0\sqrt{\Omega_{\text{rad}}a^{-4} + (\Omega_{\text{DM}} + \Omega_{\text{bar}})a^{-3} + \Omega_\Lambda a^{-3(1+w)} + \Omega_k a^{-2}}. \tag{1.12}$$

When the scale factor $a(t_0) = 1$, then $w(a)$ is equal to w_0. Currently, the curvature of space k is zero and the radiation density parameter can be neglected. For the Hubble parameter therefore applies

$$H(a) = H_0\sqrt{(\Omega_{\text{DM}} + \Omega_{\text{bar}})a^{-3} + \Omega_\Lambda + \Omega_k a^{-2}}. \tag{1.13}$$

In the present Universe (t_0), classical matter, dark matter, dark energy and space curvature density parameters are bound by relationship

$$\Omega = \Omega_{\text{bar}} + \Omega_{\text{DM}} + \Omega_\Lambda = 1 - \Omega_k, \tag{1.14}$$

where Ω is the total energy density parameter.

Ω	k	geometry	Universe	angles of triangle
< 1	> 0	spherical	closed	$> 180°$
$= 1$	$= 0$	flat	flat	$180°$
> 1	< 0	hyperbolic	open	$< 180°$

Table 1.1: The space curvatures, geometries, types of the Universe and sums of angles of a triangle for different values of total energy density parameter.

   The geometries and types of the Universe for three different values of Ω are listed in Table 1.1. Figure 1.3 shows the dependency of the expansion rate on total matter Ω_m ($\Omega_{\text{bar}} + \Omega_{\text{DM}}$) and dark energy Ω_Λ density parameters. The expansion rate (or collapse rate) determines the possible type of "death" of the Universe. Accelerate expanding open Universe may end up by so-called "Big Rip" – if the expansion accelerates forever, one day it can be so strong, it might beat the gravity and other forces and it might rip the Universe apart. For flat Universe, there is the "heat death" which should occur in around 10^{14} and more years. After so long time all the stars and even the black holes will vaporize and the Universe will be in very high entropy state. For closed Universe with no dark energy and overcritical density of matter, the most probable type of death is the "Big Crunch" which is sort of opposite event to the "Big Bang".
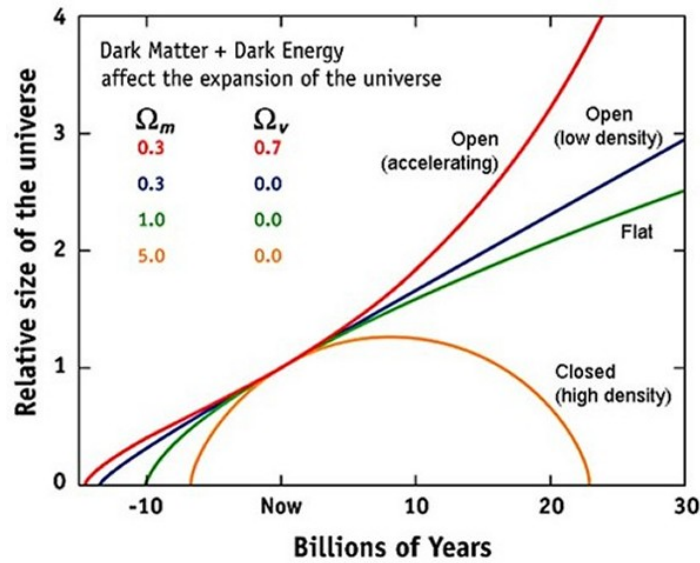
Figure 1.3: The shape of the Universe for different values of dark matter and dark energy density parameters (Physicsoftheuniverse 2009). The Universe with dark matter ($\Omega_m = 0.3$) and dark energy ($\Omega_\Lambda = 0.7$) is an accelerate expanding open Universe. Universes with no dark matter and $\Omega_m < 1$ are decelerate expanding open Universes. For Universe with $\Omega_m = 1$ the expansion ends in an infinite amount of time and such Universe is flat. When the density parameter of matter is higher than 1, the Universe is closed and recollapses.

1.3 Cosmological constraints

The density parameters and the Hubble constant are the main cosmological quantities. Some of them may be estimated from studying the clusters of galaxies and comparing the observations to computer simulations. Currently we are not able to estimate the values precisely, but we can lay down the constraints to certain cosmological parameters. Some of the parameters and their values are listed in the Table 1.2. The values were obtained by combining several methods and searching the intersection as shown in the Figure 1.4.

Parameter	Value
Ω_Λ	0.725 ± 0.016
Ω_{DM}	0.229 ± 0.015
Ω_{bar}	0.0458 ± 0.0016
Ω	1.000 ± 0.022
H_0 [km s^{-1} Mpc^{-1}]	70.2 ± 1.4
t_0 [Gyr]	13.76 ± 0.11

Table 1.2: Average values of cosmological parameters from WMAP+BAO+H_0 for flat ΛCDM cosmology (Komatsu et al. 2011).
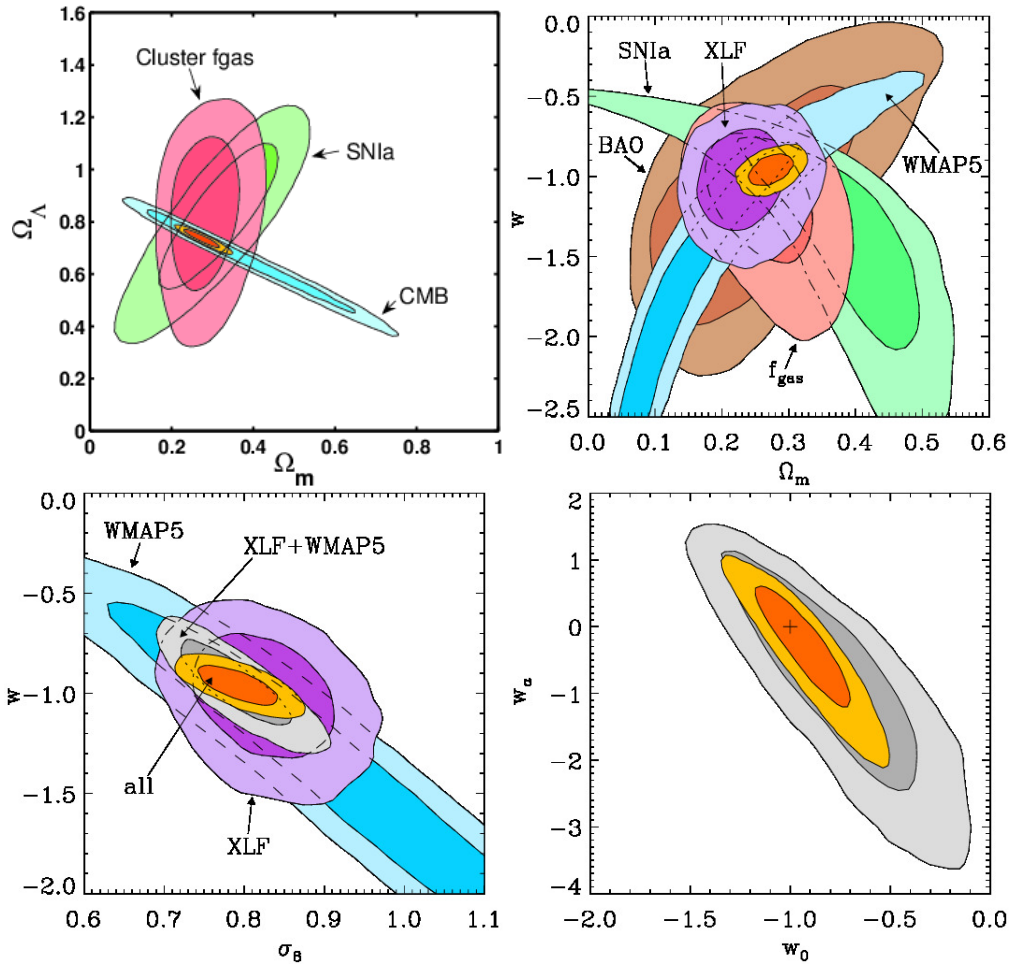
Figure 1.4: Constraints to cosmological parameters obtained by composition of different methods of measurements: gas fraction (f_{gas}), Baryon Accoustic Oscilations (BAO), Cosmic Microwave Background (CMB), X-ray Luminosity Function (XLF), Five-Year WMAP results (WMAP5) and SuperNovae type Ia (SNIa) (Allen et al. 2011).

2. Galaxy Clusters

Galaxy clusters, as the name suggests, are large groups of galaxies. They might consist of up to thousands of galaxies (mostly faint dwarf galaxies). In distant clusters, only about hundreds of galaxies are luminous enough to be seen optically. The rest of the clusters matter can be observed in the X-ray part of the spectrum or detected indirectly by the gravitational lensing or the inverse Compton scattering of the CMB photons (further described in Section 2.2). The biggest clusters have a few megaparsecs across and the typical mass of such cluster is $10^{14} - 10^{15}$ solar masses. The closest and best known clusters are the Coma cluster, Virgo cluster, Perseus cluster, Bullet cluster (shown in Figure 2.1) and Abell 1689.

Galaxy clusters are composed of the classical baryonic matter (stars, hot intracluster medium, active galactic nuclei etc.), dark matter and dark energy. The optically visible (stellar) matter accounts from 6 % up to 24 % (Laganá et al. 2008) of all the baryonic matter in the cluster. The stellar-to-gas mass ratio depends on temperature and decreases for higher temperatures. The remaining baryonic matter can be either visible in X-rays (intracluster medium) or not visible at all (cold gas). Baryonic matter makes up only less than about one-sixth ($7 - 15$ %; Laganá et al. 2008) of all the matter in the cluster, the rest of matter is in the form of dark matter.
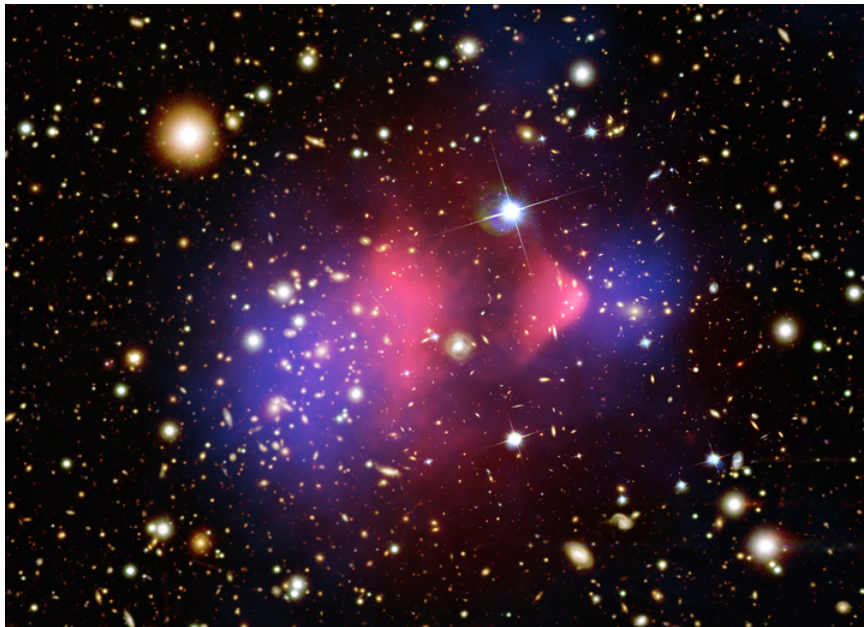

Figure 2.1: Image of the Bullet cluster composed from X-ray (Markevitch 2006) and optical (Clowe et al. 2006) images and the gravitational lensing map (Clowe et al. 2006). The pink regions correspond to the hot intracluster medium, the violet regions to halos of dark matter and each yellow object is the single galaxy.

Intracluster medium (ICM) is basically a hot intergalactic plasma, that accounts for most of the baryonic matter in the cluster. It is mostly ionized hydrogen heated to temperatures up to hundreds of megakelvins due to thermal bremsstrahlung. Classical galaxy cluster's ICM is heated to temperatures around 10^8 K. For smaller clusters, the temperature is lower (10^7 K). At such high temperatures, the plasma emits electromagnetic radiation at X-ray energies.

The X-ray emission of the ICM gave an explanation of part of the missing mass of clusters and allows the detection of clusters out to $z > 1$. Measurements of ICM temperatures also gave an independent confirmation of dark matter existence. It proofed that the gravitational potential of clusters should have an additional dark matter component. Free electrons in ICM are responsible for inverse Compton scattering of the cosmic microwave background (CMB) photons. So also the distortions of the CMB spectrum is a result of dark matter existence (edited from Kravtsov & Borgani 2012).

2.1   Properties of galaxy clusters

Primary cluster properties are the total mass, total size and temperature of the intracluster medium. The secondary parameters are: star-to-gas and gas-to-total mass fractions, density profiles of both components, radial velocity profiles and profile of metalicity. Other parameters as pressure, electron density or entropy can be derived from them.

Instead of the total mass which is in substance impossible to determine since clusters are not exactly bounded, is often used the so-called virial mass. It is defined as the mass of the central region of the cluster, where the mean density reaches the critical density multiplied by the overdensity parameter:

$$M_{\text{vir}} = \frac{4\pi}{3} r_{\text{vir}}^3 \Delta_{\text{c}} \rho_{\text{crit}}, \tag{2.1}$$

where Δ_{c} is the overdensity parameter and r_{vir} is the virial radius. The value of the overdensity parameter can be obtained from the formula by Bryan & Norman (1998)

$$\Delta_{\text{c}} = 18\pi^2 + 82[\Omega(z) - 1] - 39[\Omega(z) - 1]^2, \tag{2.2}$$

where $\Omega(z)$ is the total energy density parameter at redshift z. The overdensity parameter in flat Universe is equal to ≈ 177.65, however typically is adopted the value 200 and parameters M_{200} and r_{200} are referred to as the virial mass and the virial radius.

The gravitational interaction from the cluster can be expressed by the virial velocity

$$V_{\text{vir}}^2 = \frac{GM_{\text{vir}}}{r_{\text{vir}}}, \tag{2.3}$$

where G is the gravitational constant. The virial velocity decreases the radial velocity of the cluster from the value calculated for corresponding distance d by Hubble's law:

$$v_r(d, z, M_{\text{vir}}) = H(z)d - 0.8V_{\text{vir}} \left(\frac{r_{\text{vir}}}{d}\right)^{n_{\text{vir}}}, \tag{2.4}$$

where n_{vir} is the power-law index which determines the slope of the density profile, and v_r is the measured radial velocity of the cluster. The power-law index should in general depend on the mass of the cluster M_{vir} and redshift z, but often it is approximated by constant value valid within a certain range (equations taken from Lee et al. 2015).

The density distribution of dark matter is most often described by the Navarro, Frenk & White (NFW) profile (Navarro et al. 1995)

$$\rho_{\text{DM}}(r) = \rho_{\text{crit}} \frac{\delta_c}{r/r_s \left(1 + r/r_s\right)^2}, \tag{2.5}$$

where $r_s = r_{200}/c$ is the characteristic radius and δ_c and c are dimensionless parameters describing the concentration of the halo. The δ_c parameter is conditioned by the requirement that within radius r_{200} the mean density of the halo is $200 \times \rho_{\text{crit}}$ and therefore for δ_c applies the formula

$$\delta_c = \frac{200}{3} \frac{c^3}{\ln(1+c) - c/(1+c)}. \tag{2.6}$$

The NFW profile well describes the dark matter density distribution in cluster halos, but the profile of the ideal gas is better expressed by the empirical beta model (Jones & Forman 1984) which has higher value of the exponent than the NFW profile and therefore is shallower in the central parts. For the beta profile of the isothermal gas applies the formula

$$\rho_{\text{gas}}(r) = \rho_0 \left[1 + \left(\frac{r}{r_c} \right)^2 \right]^{-3\beta/2}, \tag{2.7}$$

where ρ_0 is the density in the center, r_c is the core radius and β is the isothermal exponent. The value of the β parameter lies near $\approx 2/3$ for most clusters (Jones & Forman 1984).

There is plenty of similar profiles which tend to describe the gas distributions in halos of galaxies and clusters. In the practical part we used the Dehnen's (Dehnen 1993) and Hernquist's (Hernquist 1990) profiles (further described in Chapter 3), when generating the initial conditions, and then we used the NFW and beta profiles, when comparing the results.

Since the gas density is not the directly measurable quantity, we have to find another quantity, that we can compare the profile with. Such quantity is the electron density $n_{\text{e}}(r)$ which can be derived from the spectral analysis of X-ray measurements of the ICM. Electron density can be expressed from the density of gas by the relationship

$$n_{\text{e}}(r) = \frac{\rho_{\text{gas}}(r)}{\mu m_{\text{p}}}, \tag{2.8}$$

where m_{p} is the mass of a proton and μ is the mean molecular weight which is, in general, function of metallicity. For simplicity we use the constant value of μ and therefore the electron density is only directly proportional to the density of gas.

Next relevant property of the ICM is its temperature profile. Temperature is a directly measurable quantity and can be derived from the spectroscopy of the cluster. With knowledge of temperature profile and electron density profile we can now compute other important parameters of the cluster: pressure profile $P(r)$ and specific entropy profile $s(r)$ (entropy per particle). For pressure of the ideal gas in the hydrostatic equilibrium applies

$$P(r) = n_{\text{e}}(r) k T(r), \tag{2.9}$$

where k is the Boltzman's constant. From the pressure profile, some interesting properties of the ICM, such as shock and cold fronts, can be discovered. Even better quantity for observation of the features in the ICM is the specific entropy which also records the history of changes. The specific entropy s is as well as pressure proportional to both temperature and electron density

$$s = \frac{1}{\gamma - 1} k \ln \left(\frac{P}{\rho^\gamma} \right) = \frac{1}{\gamma - 1} k \ln \left(\frac{T}{\rho^{\gamma-1}} \right), \tag{2.10}$$

where γ is the adiabatic coefficient and for ideal gas is equal to $5/3$. Instead of the specific entropy is often used the entropy parameter A (notation from Springel 2005b) which is only a function of specific entropy

$$A(s) = \frac{kT}{n_{\text{e}}^{2/3}}. \tag{2.11}$$

The entropy function is rather used mainly because of the non-logarithmic slope.

2.2 Observation of galaxy clusters

As said before, in the galaxy cluster we can visually (with classical optical detectors and telescopes) observe only big and bright galaxies. The remaining part of the matter must be observed on other parts of spectra or indirectly. The observations are done mostly with huge and most modern telescopes and probes provided by European Space Agency (ESA) and American National Aeronautics and Space Administration (NASA). Using these observations and measurements we can determine important cluster properties and estimate some of the cosmological constraints.

Optical observations

The major part of the visible light (mainly starlight) from a cluster comes from the largest galaxies. These galaxies have mostly elliptical or lenticular shape and are located in central regions of the cluster. Such observations can be used for estimation of the minimal mass of the cluster. Other properties that can be determined are the profiles of electron density, luminosity or radial velocity. We can also use the spectral information (redshift) to estimate the distance of the cluster.

The optical observations might also have some disadvantages. Undesirable projection effects might occur. Or some optically luminous and rich clusters may not have especially high mass and vice versa – clusters, that are not very optically active may be quite heavy.

The basic optical observations of galaxy clusters, or more accurately of big galaxies in their center, can be obtained even by amateur astronomers (Figure 2.2). Such measurements can be used for estimations of the brightness profile and total luminosity. More information can be derived from the optical spectroscopy, from which we can determine the radial velocity, distance or velocity dispersion of the cluster. For high resolution and high signal-to-noise spectra are needed the biggest telescopes and most modern spectroscopes such as *Gemini*, *VLT* or *LAMOST*.

X-ray observations

Cluster halos are filled with DM and baryonic particles. Classical baryonic particles are there in the form of diffuse gas (intracluster medium). This gas is heated to very high temperatures ($10^7 - 10^8$ K) due to the high gravitational potential of a cluster . When such particles collide, they emit high energy photons such as X-rays. The X-ray emission is mostly caused by bremsstrahlung (free-free emission) and is proportional to the square of electron density and to the square root of temperature. The electron density varies from 10^{-5} cm^{-3} at cluster's edges to 10^{-1} cm^{-3} at its center. For such low densities, the plasma is optically thin (Allen et al. 2011).

X-ray observations are less prone to projection effects. But the detection of clusters using X-ray is still not based on mass measurements. Using high resolution spatially resolved spectra of a cluster the density, temperature or metalicity profiles of the ICM can be determined. The observations of clusters at X-ray energies are provided by special spacecrafts by NASA and ESA and one of the best known are *ROSAT*, *Chandra* or *XMM-Newton*.

Gravitational lensing

Another method for observation of clusters of galaxies is the weak and strong gravitational lensing. The gravitational lensing uses the fact that the enormous mass of the cluster bends the light of galaxies from behind the cluster. The more massive the cluster is the more it bends the light. Such measurements are mass-based and give us the information about total mass of the cluster.

The observations of clusters using the strong gravitational lensing is very observably demanding. Some galaxies might be projected twice or even more times and we mostly can not even see

the original appearance of the galaxy. For this reason is rather used the weak gravitational lensing which examines if the appearance of background galaxies is stretched in some preferred directions. Using this method was determined the lensing map from Figure 2.1.

2.3 Virgo cluster

The Virgo cluster is one of the nearest and one of the biggest known galaxy clusters. In the night sky it is projected in the Virgo constellation. The Virgo cluster and the Local Group[1], are both part of a larger structure called the Virgo supercluster. The Virgo cluster consists of more than 2000 galaxies, most of which are dwarf and not very bright galaxies. The center of the cluster consists of large elliptical galaxies, the most massive are M87, M86 and M84 which can be seen in the Figure 2.2. The size of the Virgo cluster is in the order of a magnitude as the size of the Local group, but contains about 50 times more galaxies.

Figure 2.2: The optical image (mosaic) of the Virgo cluster obtained by astrophotographer Rogelio B. Andreo (2011) showing the central regions with biggest and brightest galaxies. The field of view is $5 \times 3^\circ$.

The Virgo cluster is so massive, the Local group actually experiences its gravitational pull in the form of a *Virgocentric flow*. The *Virgocentric flow* is an excess of the radial velocity of galaxies in the Virgo cluster from the value computed for corresponding distance by Hubble's law. The center of the Virgo cluster is moving away from us at speed of around 200 km s^{-1} lower than it is expected (Chernin et al. 2010).

According to the Tolman-Bondi model (Bondi 1947) the distance of the Virgo cluster is more than 15 megaparsecs (15.4 ± 0.4 Mpc; Fouqué et al. 2001). The value obtained by the Tully-Fisher method (Tully & Fisher 1977) is slightly higher 18.0 ± 1.2 Mpc (Fouqué et al. 2001). First estimations of mass of the cluster (around $10^{14} M_\odot$) have already been done in the 1930s by Sinclair Smith (1936). Current estimations lie within an order of a magnitude to that value (depending on the used method). The value obtained from the Tolman-Bondi model is $1.2 \times 10^{15} M_\odot$ within 8 degrees

---

[1]Local Group is the group of galaxies consisting of our Galaxy, the Andromeda galaxy, both Magellanic clouds and hundreds of nearest dwarf galaxies.

(2.2 Mpc for distance 15.4 Mpc) from the center of the cluster (Fouqué et al. 2001) which is 1.7 of the virial mass computed from the radial velocity recession by the relation given by Tully & Shaya (1984). The newest estimations of the Virgo cluster's mass were acquired from radial velocity profiles of filament galaxies and are very close to value from the Tolman-Bondi model. Lee et al. (2015) calculated the dynamical mass of the cluster and found the value $0.84 \, ^{+2.75}_{-0.51} \times 10^{15} \, h^{-1} M_{\odot}$.

The mass of the M87 sub-cluster estimated from the X-ray emission measured by *ROSAT* probe is $\sim 1 - 6 \times 10^{14} M_{\odot}$ within 5 degree radius from the cluster's center (Böhringer et al. 1994). The masses of M49 and M86 sub-clusters ($\sim 10^{13}$) can be neglected. Urban et al. (2011) analyzed the data of the Virgo cluster's ICM from the *XMM-Newton* and from the mass-temperature relation obtained the value $1.4 \times 10^{14} M_{\odot}$. The discrepancy between estimations obtained from radial velocity and the X-ray emission of the ICM has not been explained yet. The image of the Virgo cluster's intracluster medium taken by *ROSAT* is shown in the Figure 2.3. The mean temperature of the ICM is 2.7×10^7 K (Urban et al. 2011). The profiles of temperature and other quantities are shown in the practical part (Chapter 4).
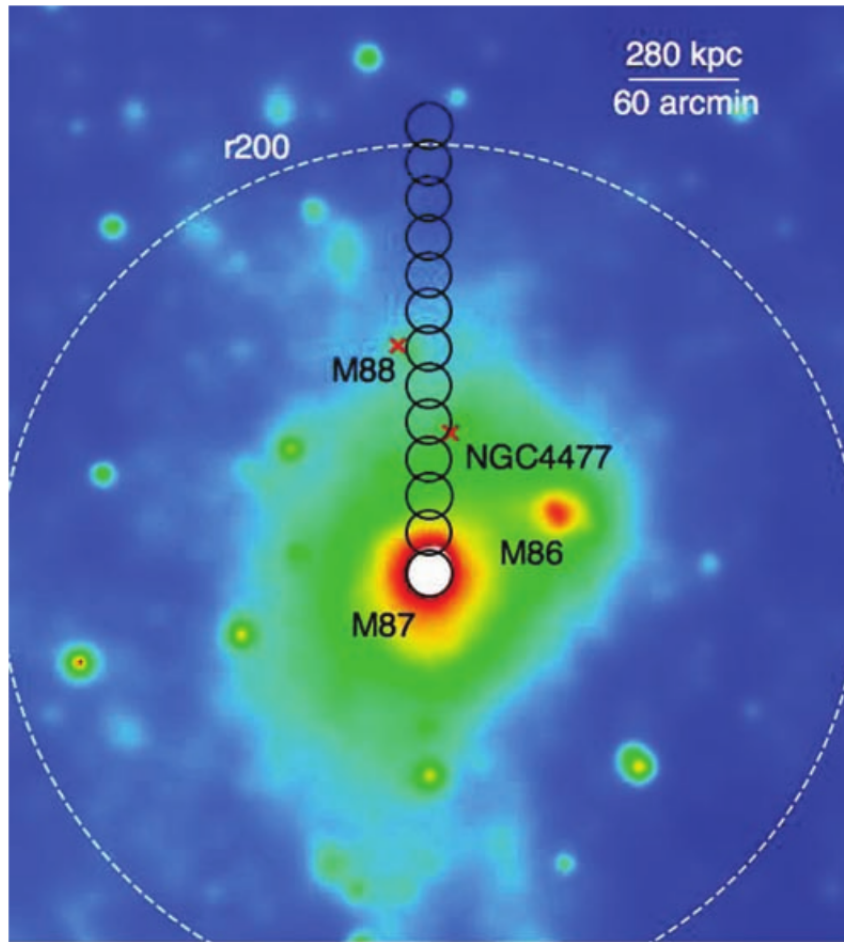

Figure 2.3: X-ray image of the Virgo cluster from the *ROSAT* telescope (the bandwidth is $0.5 - 2.0$ keV). The black circles are the regions, where the cluster was observed by the *XMM-Newton*. The measurements were latter used for the spectroscopy of the cluster by Urban et al. (2011). The white dashed line corresponds to the virial radius r_{200} determined from the mass-to-temperature scaling relations to 1.08 Mpc (3.9 degrees).

3. *Gadget-2*

Gadget-2 (GALaxies with Dark matter and Gas intEracT) is a free available N-body cosmological code for numerical computer simulations written by Volker Springel (Springel 2005*b*). It is basically an improved version of *Gadget* (Springel et al. 2001). Both versions of the *Gadget* code are widely used by the professional community for simulating clusters of galaxies or making the Millennium simulations. Currently, a new version called *Gadget-3* is being developed.

Gadget-2 is a cosmological TreeSPH code. It can be used for collisionless fluid N-body simulations or even for ideal gas simulations (smoothed particle hydrodynamics). Gravitational forces as well as hydrodynamical equations are computed approximatively. Long-range forces are computed using Fourier techniques and for short-range forces the tree particle mesh (TreePM) method is used. For faster course of the simulation, the system is decomposed into parts and every part is computed by single processor. The decomposition is realized by the Peano-Hilbert curve (further described in Section 3.3) which is afterwards cut into domains (Springel 2005*b*).

The code is written in C language and is fully portable across all UNIX systems. The code uses the following open-source libraries: GNU Scientific Library (GSL), Fastest Fourier Transform in the West (FFTW) and, if needed, also the Hierarchical Data Format (HDF5) which should be compiled with parameters recommended by the User guide (Springel 2005*c*). The code itself also has to be compiled using the makefile, where the parameters for an appropriate simulation must be chosen. The *Gadget-2* code also uses an explicit communication model that is implemented with the standardized Message Passing communication Interface (MPI), so the code can be run on both huge clusters of workstations or on individual PC's.

3.1 Simplified dynamics

If we would want to compute precisely the dynamics of a system with millions and more particles, it would be very time-consuming. If we include only gravitational forces, we would have to calculate gravitational pull from all particles to every other particle. Such a sum would have $N(N-1)$ members. The *Gadget-2* code, therefore, uses simplified dynamic and hydrodynamic equations in its numerical simulations. When simulating halo's made purely of dark matter, only the collisionless dynamics is used. For ideal gas simulations, there is the smoothed particle hydrodynamics (SPH). For a mixture of DM and ideal gas, the code uses both collisionless dynamics and SPH.

These simplifications cause the force computations to be slightly inaccurate. But fortunately errors up to 1 %, when they are randomly distributed, cause only a minimal precision loss in the resulting dynamics of the system. They also tend to slightly increase the numerical relaxation rate (Hernquist et al. 1993).

Collisionless dynamics

The dynamics of halo's of dark matter particles is described by the Friedman-Lamaître model (described in Chapter 1). For N tracer particles the Hamiltonian is

$$H = \sum_i \frac{\mathbf{p}_i^2}{2m_i a(t)^2} + \frac{1}{2} \sum_{ij} \frac{m_i m_j \, \varphi(\mathbf{x}_i - \mathbf{x}_j)}{a(t)}, \tag{3.1}$$

where $a(t)$ is a time dependent scale factor, $\mathbf{x}_i$ are comoving coordinates, $\mathbf{p}_i = m_i \dot{\mathbf{x}}_i a^2(t)$ are corresponding momenta and $\varphi(\mathbf{x}_i - \mathbf{x}_j)$ is the gravitational potential. Due to time dependence of the scale factor the Hamiltonian also varies in time.

For periodic boundary conditions of L^3 cube the potential is described by the Poisson equation

$$\nabla^2 \varphi(\mathbf{x}) = 4\pi G \left(\sum_n \tilde{\delta}(\mathbf{x} - \mathbf{n}L) - \frac{1}{L^3} \right), \tag{3.2}$$

where $\tilde{\delta}$ is Dirac δ-function. Using peculiar potential $\phi(\mathbf{x}) = \sum m_i \varphi(\mathbf{x} - \mathbf{x_i})$ we can rewrite (3.2) into the form where matter density occurs

$$\nabla^2 \phi(\mathbf{x}) = 4\pi G \left(\rho(\mathbf{x}) - \bar{\rho} \right), \tag{3.3}$$

where $\bar{\rho}$ is a mean matter density.

In *Gadget-2* simulations the Dirac δ-function is convolved with a gravitational softening kernel $\tilde{\delta}(\mathbf{x}) \approx W(|\mathbf{x}|, 2.8\varepsilon)$ – the spline kernel of comoving scale ε by Monaghan & Lattanzio (1985) is used:

$$W(r, h) = \frac{8}{\pi h^3} \begin{cases} 1 - 6\left(\frac{r}{h}\right)^2 + 6\left(\frac{r}{h}\right)^3, & 0 \le \frac{r}{h} \le \frac{1}{2}, \\ 2\left(1 - \frac{r}{h}\right)^3, & \frac{1}{2} \le \frac{r}{h} \le 1, \\ 0, & \frac{r}{h} > 1, \end{cases} \tag{3.4}$$

where h is the gravitational softening length. So according to (3.4) the gravity only effects on distances up to h, more distant objects do not gravitationally interact (equation taken from Springel 2005*b*).

Smoothed particles hydrodynamics

The *Gadget-2* code uses discrete tracer particles in its SPH equations to describe the state of a fluid. The particles are characterized by their position $\mathbf{r}_i$, velocity $\mathbf{v}_i$ and mass m_i. The density estimate for such particles is described by the SPH softening kernel (3.4):

$$\rho_i = \sum_{j=1}^{N} m_j W(|\mathbf{r}_i - \mathbf{r}_j|, h_i), \tag{3.5}$$

where h_i is the adaptive softening length – the value of the softening length changes so the volume with radius h_i contains constant mass and obeys the equation

$$\frac{4\pi}{3} h_i^3 \rho_i = N_{\text{sph}} \bar{m}, \tag{3.6}$$

where N_{sph} is the typical number of neighbours and $\bar{m}$ is the average mass. The typical number of SPH neighbours is 35.

The thermodynamic properties of particles may be described by its thermal energy per unit mass u_i or by entropy per unit mass s_i. For reasons discussed in Springel & Hernquist (2002) the *Gadget-2* (mainly because of entropy conservation) rather uses the entropy per unit mass s_i as the independent variable. And rather than the specific entropy (entropy per unit mass) is used the entropy function $A(s) = P/\rho^\gamma$. For equations of motion applies

$$\frac{\mathrm{d}\mathbf{v}_i}{\mathrm{d}t} = -\sum_{j=1}^{N} m_j \left[f_i \frac{P_i}{\rho_i^2} \nabla_i W_{ij}(h_i) + f_j \frac{P_j}{\rho_j^2} \nabla_i W_{ij}(h_j) \right], \tag{3.7}$$

where P_i is pressure and f_i is defined as

$$f_i = \left(1 + \frac{h_i}{3\rho_i} \frac{\partial \rho_i}{\partial h_i} \right)^{-1}. \tag{3.8}$$

For entropy discontinuities generated by microphysics the artificial viscosity is introduced and is further described in Springel & Hernquist (2002).

3.2 Running *Gadget* using several CPU's

Some of most modern supercomputers so-called vector machines are able to provide simultaneous computations on whole arrays of numbers which would the best for computing the evolution of a N-body system. Unfortunately most of algorithms are not able to fully use the capabilities of such machines and they are better used on scalar architectures. On scalar architectures there is mostly the problem with high computing time and memory, because most software's and codes can run only on a single processor.

To make the algorithm effective we need to decompose the problem into parts and let each processor do computations for each part. The Symmetric MultiProcessing (SMP) computers are really good for that. The SMP's consists of several classical scalar processors, but they share the main memory, so the computations are distributed much more easily. For classical computers without shared memory the more radical parallelization is used – each scalar processor is treated as an independent computer and runs a separate instance of code.

There are many methods for decomposing a 3D problem – often used was the hierarchical orthogonal bisection, but this method has many disadvantages. Main disadvantage is that particles will experience different force error with different number of processors used. The *Gadget-2* code rather uses the Peano-Hilbert curve and then cuts this curve into domains (as Figure 3.1 shows). Each domain is then computed a by single scalar processor. The Peano-Hilbert curve is an one dimensional curve that entirely fills higher dimensional spaces. This method brings particles after each domain decomposition into the Peano-Hilbert order which improves cache utilization and performance of the code (Springel 2005*c*).

Thanks to the Multi Passing Interface (MPI) we are able to start the *Gadget-2* code using multiple processors on the same computer or even on multiple computers. The code can therefore be run on a single notebook (small collisionless simulation) or on massively parallel computers with distributed memory (huge SPH simulations) (edited from Springel 2005*b*).
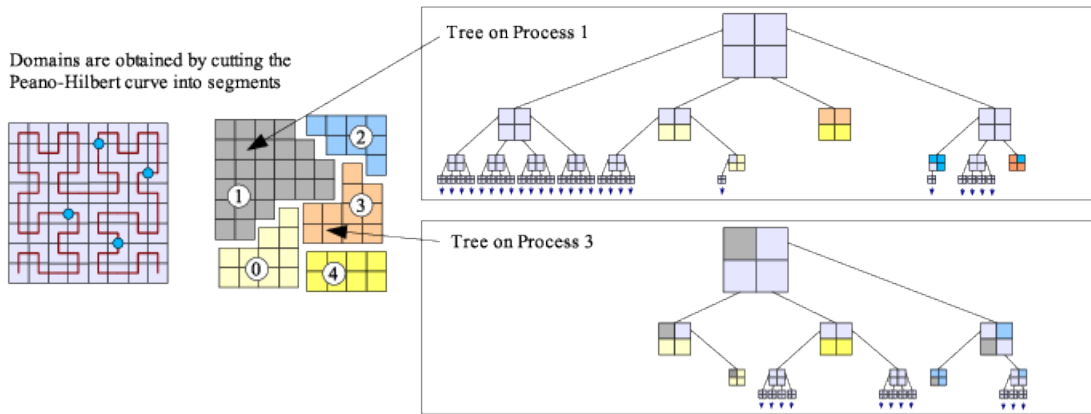
Figure 3.1: Domain decomposition of the Peano-Hilbert curve. Each domain is computed by single processor (picture taken from Springel 2005*b*)

.

3.3   Initial conditions

One of the most important things when simulating a cluster (or when making any other simulation) are the initial conditions – density, temperature and velocity distributions of particles. If we have totally wrong initial conditions we can change the simulation parameters in any possible way but we will never get a model that has similar properties as our cluster. For generating the initial conditions for a Virgo cluster simulation we used the initial conditions generator called *Clustep* (Ruggiero 2013).

3.3.1   *Clustep*

Clustep is a Python script that generates initial conditions compatible with *Gadget-2*, although the produced snapshots are in *Gadget-2*'s non-default binary format (the ICFormat parameter has the value of 2). The script is compatible with both *Python-2.7* and *Python-3.5* and has to be compiled via the make command. The required libraries are *Numpy*, *Scipy*, *Matplotlib*, *Cython* and *Argparse*. The script was also used in work by Ruggiero & Lima Neto (2017).

The *Clustep* script generates a snapshot with initial conditions of a galaxy cluster in the dynamic equilibrium. The sphere of radius R is filled with mixture of gas and dark matter particles. The density profile for both ideal gas and dark matter particles is the Dehnen's density profile (Dehnen 1993)

$$\rho(r) = \frac{(3-\gamma)M}{4\pi} \frac{a}{r^\gamma (r+a)^{4-\gamma}},$$ (3.9)

where a is the scaling radius and M is the total mass and γ which is an exponent, that determines the shape of the profile especially in the central parts.

If $\gamma = 1$ the profile corresponds to the well known Hernquist's (Hernquist 1990) profile for galactic and cluster halo's. If assigned to the gas component, for $\gamma = 0$ the profile corresponds to non cool-core profile and for $\gamma = 1$ to cool-core profile. When generating the initial conditions with *Clustep*, there are four free parameters: total mass M, total radius R, scale radius a, gamma γ and optionally there is also the metalicity parameter for gas.

4. Cluster Simulations

In this chapter, we describe the usage of *Gadget-2* for galaxy cluster time evolution simulations. In Section 4.1 we show the simulation of galaxy cluster with default initial conditions (ICs) by Springel (2005*a*). The simulation contains only collisionless particles of dark matter and consequently does not provide any information about temperature, entropy nor internal energy of particles. In Section 4.2 we tried to simulate the well known Virgo cluster (properties discussed in Chapter 2). The simulation was done using a mixture of ideal gas (smoothed particle hydrodynamics) and dark matter particles (collisionless dynamics). This simulation gives the information about density, internal energy and also change of entropy of particles, so we are able to produce profiles of directly measurable quantities. The initial conditions for the Virgo cluster simulations were generated using Python script *Clustep* written by Ruggiero (2013) (described in Subs. 3.3.1).

The libraries that are required by the *Gadget-2* code (listed in Chapter 3) were compiled using parameters recommended by the User guide (Springel 2005*c*) and installed into personal directory on our university "supercomputer" called *Crab* (crab.physics.muni.cz). Before compiling the *Gadget-2* code or running the simulation the library paths must been added to the LD_LIBRARY_PATH variable. The *Gadget-2* code was compiled using the different makefile for each simulation (links to both can be found in the Appendix). In the first simulation we used the almost original Makefile – only with higher grid parameter. In the Virgo cluster simulation we made some more changes in the makefile. For the data storing we used the non-default *Gadget-2* data format – the Hierarchical Data Format (HDF5).

All the simulations were ran using the Multi Passing Interface (MPI) on multiple CPUs on *Crab*, on which we connected remotely via the ssh[1] protocol. The operating system on this computer is the classical *GNU/Debian* version 9.4, the processor is type Intel Xeon Processor E5-2630 v4 and the total number of available CPUs is 40. The usual number of CPUs used was 24 or 36 (the number of processors should be a power of two – because of the most efficient communication schemes; Springel 2005*c*) and the simulations were ran by the command

$$\$ \text{ mpirun -np 24 ./Gadget-2 parameterfile.param}$$

where parameterfile.param is a parameter-file for a specific problem (cluster simulation, millennium simulation etc.). We only used the cluster.param for spherically symmetrical simulations of clusters with vacuum boundaries.

The total CPU time varied from a few minutes for collisionless simulations to couple of hours for ideal gas SPH and dark matter simulations. The total amount of data from a single simulation depended on the number of used particles and the frequency of snapshots and varied from hundreds of megabytes (64^3 particles) to tens of gigabytes (256^3 particles) of computer memory. All the visualizations, as well as profile computations, were done in *Python 3.5* (links to scripts can be found in the Appendix).

---

[1]SSH (Secure Shell) is a secure communication protocol for computer networks.

4.1 Default *Gadget-2* cluster simulation

To demonstrate how the *Gadget-2* code works, we ran a galaxy cluster simulation with default initial conditions (IC). The IC file, we used, is named cluster_littleendian.dat[2] (Springel 2005*a*) and corresponds to the classical binary IC format – the `ICFormat` parameter has value of 1. Although the IC file is default, some changes in the parameter-file (cluster.param) were done – mainly memory allocation parameters and dynamics, SPH and time integration accuracy parameters. The link to the parameter-file can be found in the Appendix.

The simulation counts with almost $300,000$ of collisionless particles and was ran using 24 processors on the *Crab* computer. The total CPU time of the simulation was 14 hours (35 minutes per CPU) and total amount of data with 200 snapshots (for good time resolution of the simulation) was 2 gigabytes.

4.1.1 Initial conditions

There are three different types of particles (bulge, disk and halo particles) with different masses and softening lengths – this technique is called multi-mass technique (Springel 2005*c*). More detailed numbers of particles and other parameters can be found in Table 4.1. The file with initial conditions was generated with Zoomed Initial Conditions (ZIC) generator by Giuseppe Tormen (not a free available software).

Part type	Part name	Number of particles	Softening length
1	Halo	96877	500 kpc
2	Disk	39616	180 kpc
3	Bulge	140005	72 kpc

Table 4.1: Number of particles and softening lengths for used particle types.

The simulation was started at redshift $z = 23$ ($a = 0.0416$) in the box of 140 Mpc^3 of comoving coordinates with vacuum boundaries. The Figure 4.1 shows the initial particle distribution.
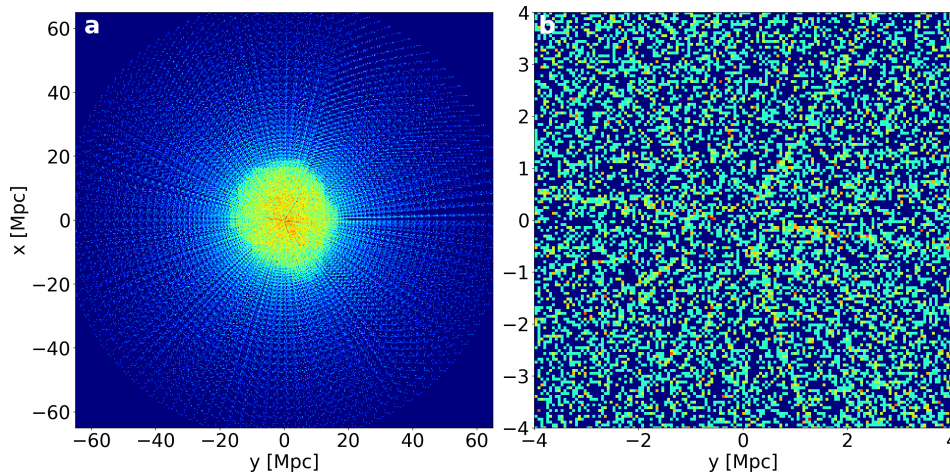

Figure 4.1: The initial density map at $a = 0.0416$ and $z = 23$. (a) The whole region with bulge, disk and halo particles. (b) The central region containing mainly the bulge particles.

---

[2]Endianness describes the order in which multi-byte numbers are stored in computer memory. Crab is the little-endian architecture.

4.1.2 Simulation

For the above showed initial conditions we ran a classical cluster simulation starting at redshift $z = 23$ up to now ($z = 0$). We used the default flat ΛCDM cosmology ($\Omega = \Omega_m + \Omega_\Lambda = 1$) and also other principal cosmological parameters (listed in table 4.2) re; unchanged. The result of the simulation is shown in the Figure 4.2.

Parameter	Value
Ω_m	0.3
Ω_Λ	0.7
Ω_{bar}	0.0
h	0.7

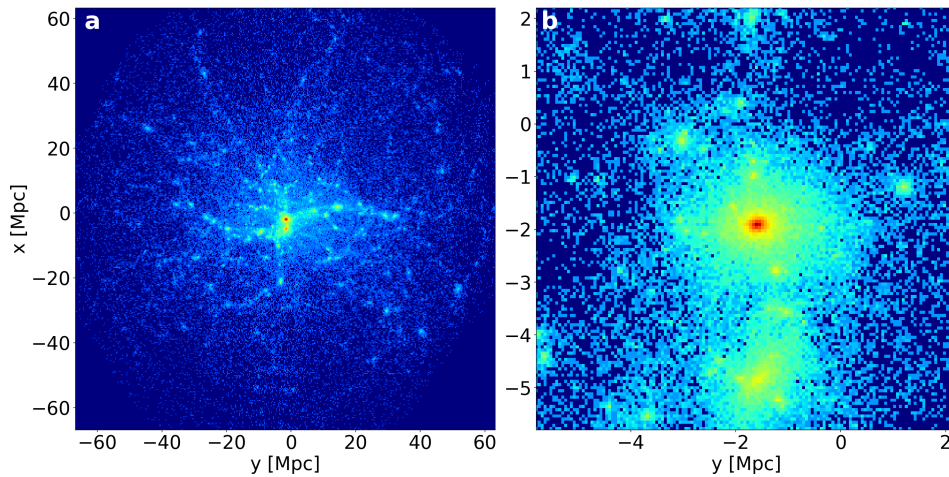Table 4.2: Cosmological parameters used in the default IC simulation.

Figure 4.2: The density map of the default IC simulation at redshift $z = 0$ ($a = 1$). (a) The whole cluster's halo with its inner structure. (b) Zoom into the central regions of the cluster where the cluster core is located.

4.1.3 Discussion

The initial density map (Figure 4.1) shows the initial layout of all three types of used particles. The distribution is spherically symmetrical and increases in the central parts. The distribution is not exactly homogeneous and isotropic; small perturbations (density fluctuations) occur.

After few crashes, mainly because of problems with tree domain decomposition, we finally found the optimal settings and the simulation ran successfully. With 24 used CPU's the simulation lasted just over 30 minutes. The result of the simulation was visualized, the final density layout is shown in Figure 4.2 and the link to full visualization (gif) of the simulation can be found in the Appendix. The visualization shows the formation of the cluster core and also of its satellite galaxies surrounding the core. The density maps were generated using 2D histogram in *Python 3.5* (*matplotlib* package).

4.2 Virgo cluster simulation

To test the functionality of the cosmological code *Gadget-2*, and also to prove our knowledge of cosmology, we attempted to produce a cosmological simulation of the Virgo cluster. Using the *Clustep* script we created own initial conditions with mixture of ideal gas and dark matter particles and ran couple of simulations. We then compared the simulations to real observations (X-ray measurements) of the Virgo cluster's intracluster medium (ICM).

The *Gadget-2* code was compiled with parameters listed in the makefile which can be found in the Appendix. The makefile is very similar to the default one which was used in the Section 4.1. Moreover we used the additional gravitational softening for gas, higher value of the grid parameter, higher resolution in the central parts and also the output of change of entropy in the snapshots.

We ran huge amount of simulations with different initial conditions (R, M, a) and cosmological parameters (Ω_Λ, Ω_0, z_i) and found the optimal ones. The fitted parameters were: the overdensity parameters R_{200}, M_{200} and the temperature profile $T(r)$. Other parameters, that we also compared, were the electron density profile $n_e(r)$, entropy parameter profile $A(r)$ and pressure profile $P(r)$. All measured profiles were taken from the *XMM Newton*'s data analysis by Urban (2011) and the virial mass is from Fouqué et al. (2001) and Lee et al. (2015). The virial radius has been computed from the virial mass using the same value of Hubble constant as used in the simulation ($H_0 = 74.02$ km s^{-1} Mpc^{-3}; Riess et al. 2019).

For the acquired initial conditions we ran a galaxy cluster simulation with 2×128^3 particles in the box of 50^3 Mpc^{-3} and therefore with high mass resolution: 4.7×10^8 $M_\odot$ per gas particle and 2.3×10^9 $M_\odot$ per dark matter particle. The simulation was ran using 36 CPU's on the *Crab* computer. The total amount of computing time was 143 hours (nearly 4 hours per CPU) and took up around 65 gigabytes of computer memory (with 300 snapshots).

4.2.1 Initial conditions

The initial conditions were generated by the *Clustep* script, the radius of the initial sphere was set $R = 25$ Mpc and the total mass $M = 5.8 \times 10^{15}$ M$_\odot$. For dark matter particles we set the cool-core profile ($\gamma = 1$) and for ideal gas we chose the non cool-core option ($\gamma = 0$). Exact values of numbers of particles, total masses and scale factors for both types of particles are listed in Table 4.3. The mean initial temperature of ideal gas was set to 4×10^6 K. The simulation was started from redshift $z = 3$ ($a = 0.25$). The initial density profile can be found in the Graph 4.3 and the initial temperature profile in the Graph 4.4. The radius scales of both graphs are logarithmic with the radii resolution 5 kpc.

Particle type	Number of particles	Total mass [M$_\odot$]	Scale factor [Mpc]	Gamma γ
Dark matter	128^3	4.93×10^{15}	12	1
Ideal gas	128^3	0.87×10^{15}	12	0

Table 4.3: Initial parameters for both types of particles.

The values of softening length parameters were set to the mean particle spacing (for uniform particle distribution) divided by the factor 35 as in Springel (2005*b*). For both types of particles the values were set to 8 kpc. For gas was also included the adaptive gravitational softening which was chosen in the makefile.
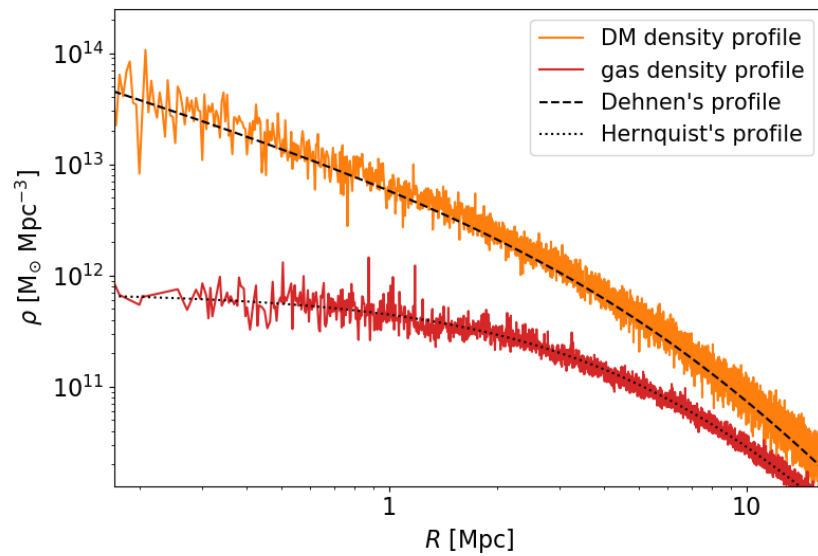
Figure 4.3: Initial density profiles of both gas and dark matter particles compared to their analytic represenations – Dehnen's profile ($\gamma = 1$) and Hernquist's profile ($\gamma = 0$).
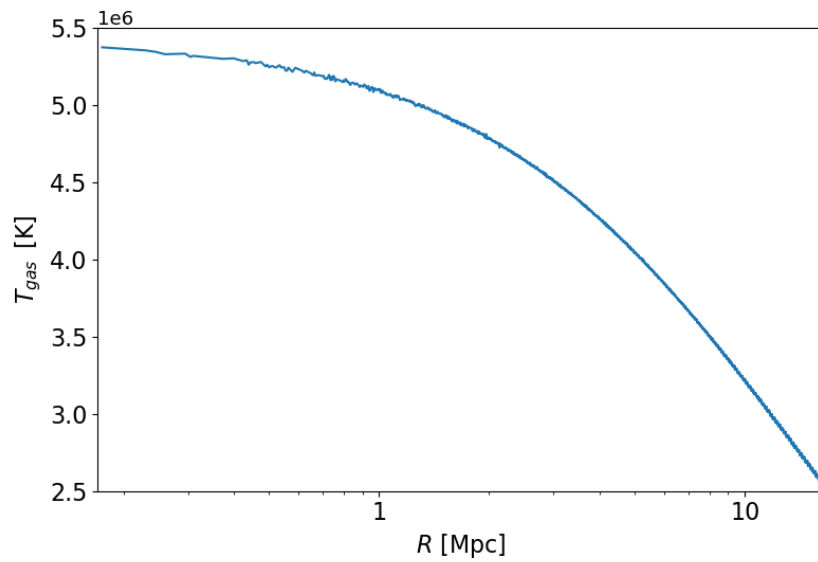

Figure 4.4: Initial temperature profile of gas in a non cool-core cluster. Mean temperature at redshift $z = 3$ is 4×10^6 K.

4.2.2 Simulation

The simulation of the Virgo cluster was ran with the initial conditions showed in the Subs. 4.2.1 and cosmological parameters listed in Table 4.4. We tried also different parameters and cosmologies, but for the flat ΛCDM cosmology ($\Omega = \Omega_\Lambda + \Omega_m = 1$) with these parameters we got the best match with the cluster's measurements. The values of main cosmological parameters were taken from NASA/IPAC Extragalactic Database (NED 2017) for the Virgo cluster and the value of Hubble constant was taken from the analysis (Riess et al. 2019) of the latest measurements of Cepheids by Hubble Space Telescope (HST). The link to the whole parameter-file can be found in the Appendix. The final density map can be found in the Figure 4.5 and the final density profile in the Figure 4.6. Profiles of other quantities compared with the measured profiles by Urban (2011) are shown in Figures 4.7, 4.8, 4.9 and 4.10.

Parameter	Value
$\Omega_{\mathbf{m}}$	0.308
Ω_Λ	0.692
Ω_{bar}	0.045
h	0.740

Table 4.4: Values of main cosmological quantities used in the Virgo cluster simulation.
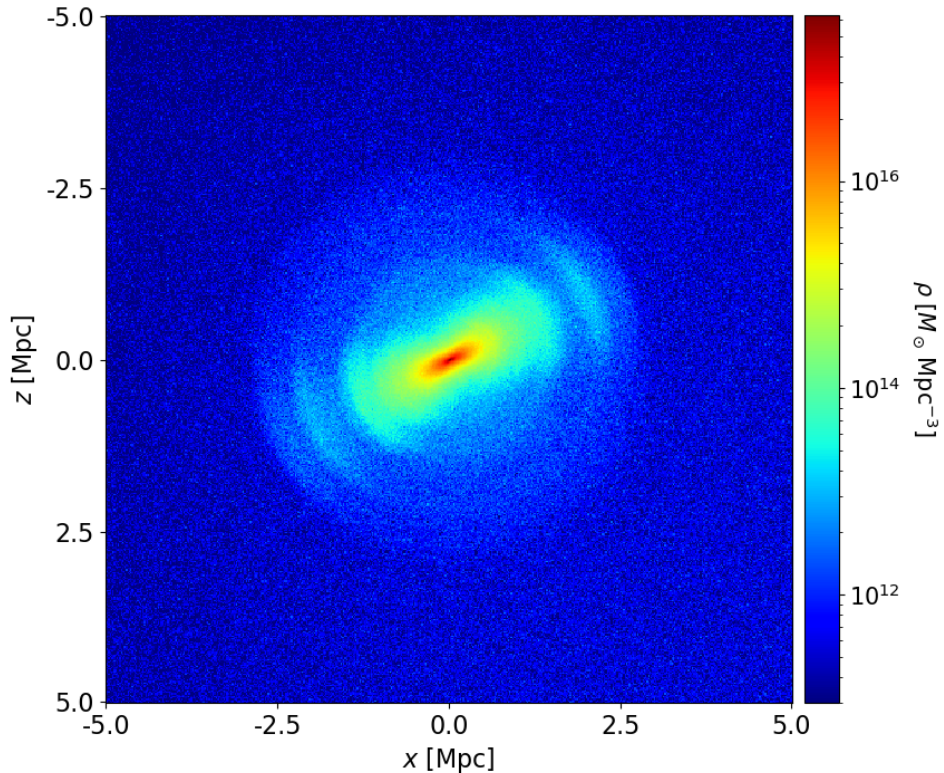

Figure 4.5: Density map of central parts of the cluster. Shells surrounding the cluster core are formed mostly from dark matter. Link to full visualization can be found in the Appendix.
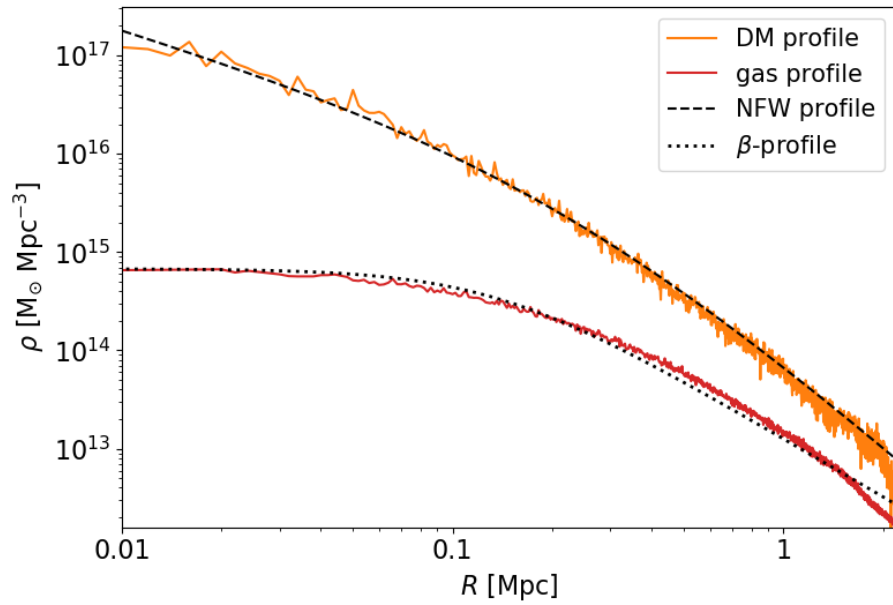
Figure 4.6: Final density profile of dark matter and ideal gas out to the virial radius $r_{200} = 2.15\,\mathrm{Mpc}$ fitted with the NFW and beta-profiles. The concentration parameter of the dark matter density profile was fitted to $c = 16.2$ and the beta parameter of the gas profile to $\beta = 0.73$.
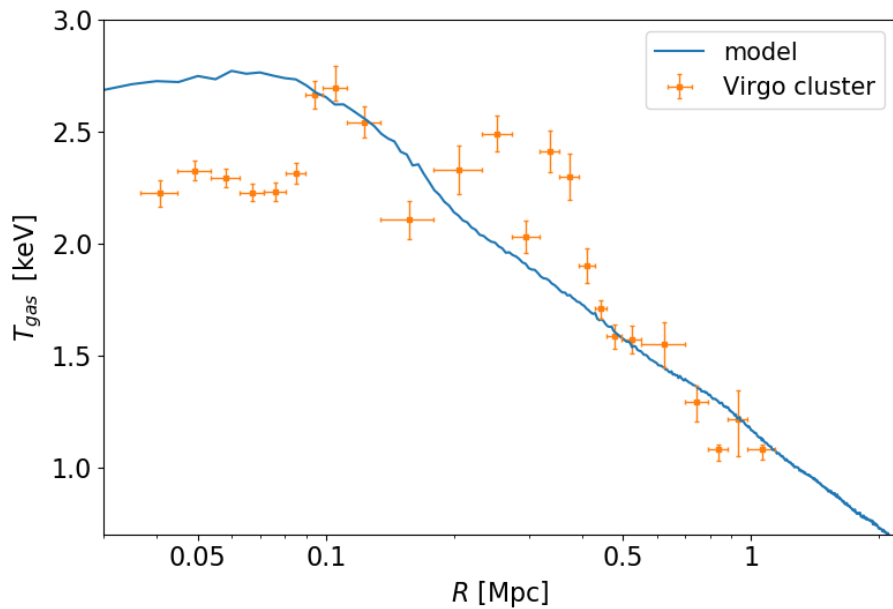

Figure 4.7: Temperature profile of ideal gas from the model compared to the measured profile of the Virgo cluster.
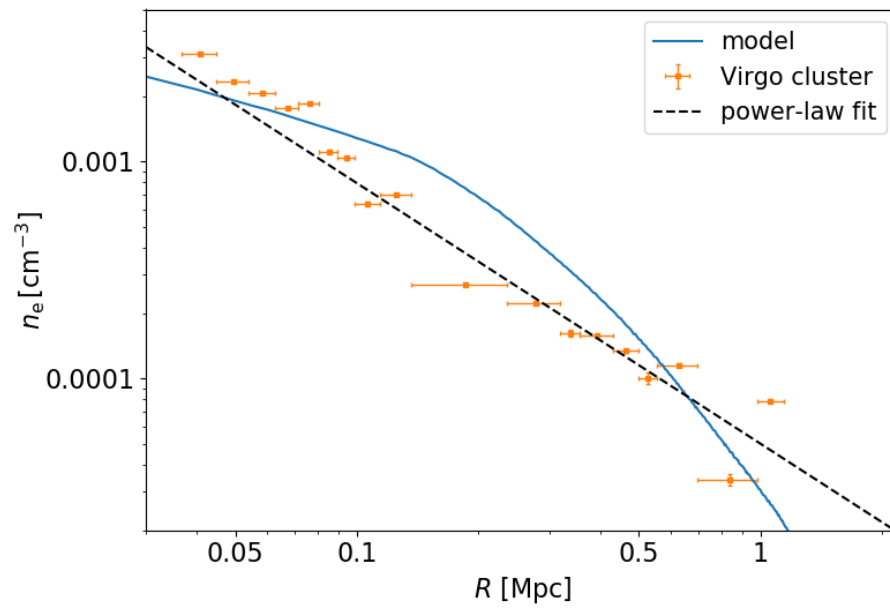
Figure 4.8: Electron density profile of ideal gas from the model compared to the computed profile of the Virgo cluster and the power-law fit (1.21 ± 0.12).
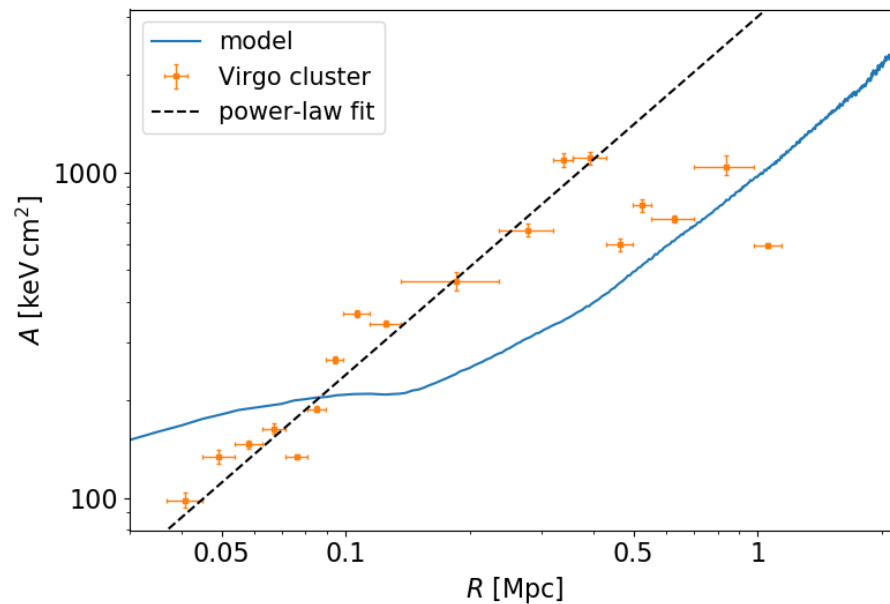

Figure 4.9: Entropy parameter $A(s)$ profile of ideal gas from the model compared to the computed profile of the Virgo cluster and the power-law fit ($\beta = 1.1$).
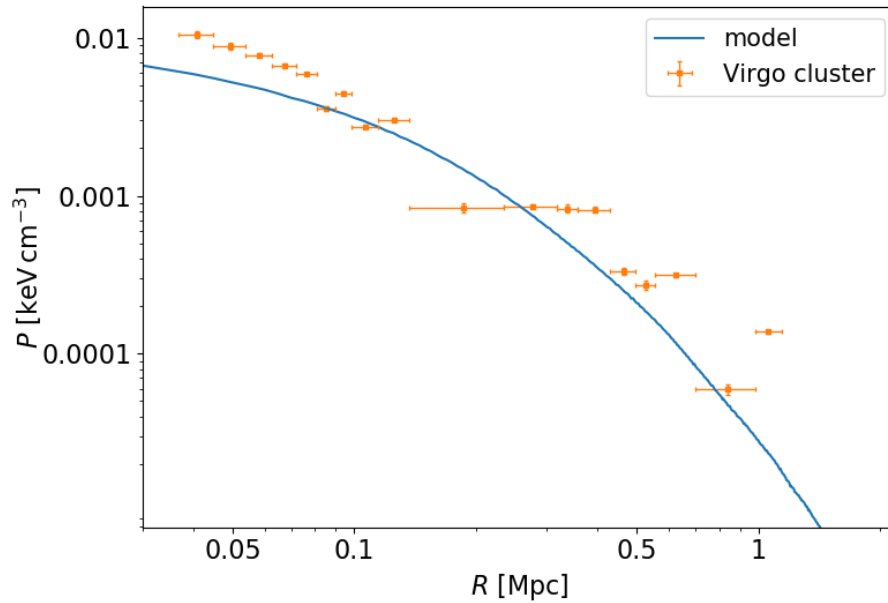
Figure 4.10: Pressure profile of ideal gas from the model compared to the deprojected measured profile of the Virgo cluster.

4.2.3 Discussion

The initial density profiles of particles from the generated IC file (Figure 4.3) fit well with their analityc profiles (Dehnen's and Hernquist's profile) and differ only due to fluctuations. The temperature profile (Figure 4.4) corresponds to the profile of a non-cool core cluster and the mean temperature is nearly 4×10^6 kelvins.

The density map in the Figure 4.5 shows the final density layout of both dark matter and ideal gas particles. The density map is zoomed into central parts of the cluster to show the density shells surrounding the cluster's core. The presence of density shells is not pretty clear. Similar shells appear at so-called shell galaxies, but their expected mechanism of creation is quite different from simple spherical collapse as in our simulation. The full visualization of the Virgo cluster simulation containing the time evolution of the density map, density profile and temperature profile is enclosed in the Appendix. As can be seen in the visualization it is mostly dark matter what forms the shells. The density profile of gas is much smoother, but shells are also included.

The final density profiles of dark matter and ideal gas were compared with NFW a beta profiles. The concentration parameters (slopes of profiles) of both components lie within an expected range. The virial mass extracted from the NFW profile $M_{200} = 1.22 M_\odot$ (virial radius 2.12 Mpc) well corresponds to the masses measured by Fouqué et al. (2001) and Lee et al. (2015). The beta parameter for gas fitted from the model ($\beta = 0.73$) lies within the standard error from the value $\beta = 0.81 \pm 0.08$ obtained by Urban (2011).

The temperature profile correlates with the measurements mainly in the outskirts of the cluster; in the central parts the measured temperature is slightly lower. The mean temperature of the model out to the virial radius is 1.9 keV and the measured is 2.3 keV (Urban et al. 2011). Profiles of electron density and entropy parameter correspond in the order to measured profiles but their slopes differ. On the other hand the pressure profile fits quite well.

Conclusion

In this thesis, we focused on cosmology, specifically on computer numerical simulations of galaxy clusters. The purposes of the thesis were to get elementary knowledge of cosmology, clusters of galaxies and their properties and to learn how to run basic cosmological simulations and compare the results with measurements of clusters.

In the theoretical part, we discussed the most important cosmological quantities and their relations. We briefly showed the use of Friedman equations in a homogeneously and isotropically expanding Universe. We then discussed the effect of density parameters on the geometry of the space. In Chapter 2, we focused on galaxy clusters. We showed how clusters can be observed and how some of the main cosmological quantities can be determined. We also took a further look at one of the best known and nearest cluster – the Virgo cluster. In the third Chapter, we revealed the cosmological code *Gadget-2* that we used for all our simulations. We mentioned its major dynamical and hydrodynamical equations and some of approximate and decomposition methods.

In the first section of the practical part (Section 4.1), we provided a galaxy cluster simulation with default *Gadget-2* initial conditions to show how this code works. We visualized the initial (Figure 4.1) and final (Figure 4.2) density map with all types of particles (halo, disk and bulge). In the final density map, we can see the densest central region which corresponds to the core of the cluster. It is often a large elliptical galaxy, as in the case of the Virgo cluster. The clumps of matter around the central parts of the cluster may correspond to satellite galaxies.

The second section of the practical part (Section 4.2) was focused on producing own initial conditions using the *Clustep* script and applying those on the Virgo cluster simulation. After huge amount of simulations, we found the optimal initial conditions (Subs. 4.2.1). The initial density profiles (Figure 4.3) of both types of particles were compared with their ideal profile. We also produced the initial temperature profile (Figure 4.4) to show that the generated cluster has a non-cool core.

With acquired initial conditions, we ran a classical galaxy cluster simulation from the cosmological redshift $z = 3$ up to now ($z = 0.0047$ for the case of Virgo cluster; NED 2017) and tried to obtain a model with properties similar to the Virgo cluster (Section 2.3). In the simulation, we used the flat ΛCDM cosmology with parameters listed in Table 4.4. The final density map showing central parts of the cluster can be found in the Figure 4.5 – the Figure shows the cluster core surrounded by shells of gas and dark matter. Similar shells can be found in halos of special types of elliptical galaxies so-called shell galaxies. In the shell galaxies the shells are though to develop after the collision with smaller galaxy (Glos 2015, Petrovská 2018). In our simulation the shells developed from spherically symmetrical collapse as the density waves of dark matter and gas particles.

The final density profiles were compared to the NFW (2.5) and beta (2.7) profiles (Figure 4.6). We also compared the profiles of main quantities that describe the intracluster medium (listed in Chapter 2) to X-ray measurements of the Virgo cluster (Urban et al. 2011). The Figures 4.7, 4.8, 4.9 and 4.10 show the temperature, electron density, entropy and pressure profiles of the ideal gas

compared to measured profiles and their power-law fits. The temperature and pressure profiles well correspond to the measured profiles. Profiles of electron density and entropy have quite different slopes than the measured ones, but they at least correspond in the order of the magnitude. However, the fits of measured profiles, especially of the entropy function profile, may look quite different for higher resolution measurements.

The constructed model is not very complex and deserves some improvements – in the first place, it could also include metalicity. For different initial conditions with more fitted parameters the conformity with measured profiles could be even better.

The main purpose of this thesis was not to acquire new estimations to some crucial cosmological parameters or properties of the Virgo cluster but to learn the basic systematics of cosmological simulations and to get the elementary knowledge of cosmology. The thesis may also be used as a guide for other students interested in cosmological simulations.

Appendix

Links

Makefiles

Default ICs – *https://is.muni.cz/auth/th/i3yrm/appendix/makefiles/Makefile_default*

Virgo cluster – *https://is.muni.cz/auth/th/i3yrm/appendix/makefiles/Makefile_Virgo*

Parameter files

Default ICs – *https://is.muni.cz/auth/th/i3yrm/appendix/params/parameters_default*

Virgo cluster – *https://is.muni.cz/auth/th/i3yrm/appendix/params/parameters_virgo*

Simulation gifs

Default ICs – *https://is.muni.cz/auth/th/i3yrm/appendix/gifs/cluster_default.gif*

Virgo cluster - *https://is.muni.cz/auth/th/i3yrm/appendix/gifs/cluster_virgo.gif*

Python scripts

2D density map - *https://is.muni.cz/auth/th/i3yrm/appendix/scripts/map.py*

Density profile - *https://is.muni.cz/auth/th/i3yrm/appendix/scripts/density.py*

Temperature profile - *https://is.muni.cz/auth/th/i3yrm/appendix/scripts/temp.py*

Electron density profile - *https://is.muni.cz/auth/th/i3yrm/appendix/scripts/electron_density.py*

Entropy profile - *https://is.muni.cz/auth/th/i3yrm/appendix/scripts/entropy.py*

Pressure profile - *https://is.muni.cz/auth/th/i3yrm/appendix/scripts/pressure.py*

References

Allen, S. W., Evrard, A. E. & Mantz, A. B. (2011), '*Cosmological Parameters from Observations of Galaxy Clusters*', Annual Review of A&A **49**, 409–470.

Böhringer, H., Briel, U. G., Schwarz, R. A., Voges, W., Hartner, G. & Trümper, J. (1994), '*The structure of the Virgo cluster of galaxies from Rosat X-ray images*', Nature **368**, 828–831.

Bondi, H. (1947), '*Spherically symmetrical models in general relativity*', MNRAS **107**, 410.

Bryan, G. L. & Norman, M. L. (1998), '*Statistical Properties of X-Ray Clusters: Analytic and Numerical Comparisons*', ApJ **495**, 80–99.

Chernin, A. D., Karachentsev, I. D., Nasonova, O. G., Teerikorpi, P., Valtonen, M. J., Dolgachev, V. P., Domozhilova, L. M. & Byrd, G. G. (2010), '*Dark energy domination in the Virgocentric flow*', A&A **520**, A104.

Clowe, D., Bradač, M., Gonzalez, A. H., Markevitch, M., Randall, S. W., Jones, C. & Zaritsky, D. (2006), '*A Direct Empirical Proof of the Existence of Dark Matter*', ApJ **648**(2), L109–L113.

Dehnen, W. (1993), '*A Family of Potential-Density Pairs for Spherical Galaxies and Bulges*', MNRAS **265**, 250.

ESA (2013), '*Planck Measurements of Cosmic Microwave Background*'.
   URL: *https://www.esa.int/spaceinimages/Images/2013/03/Planck_CMB.*

Fixsen, D. J. (2009), '*The Temperature of the Cosmic Microwave Background*', ApJ **707**, 916–920.

Fouqué, P., Solanes, J. M., Sanchis, T. & Balkowski, C. (2001), '*Structure, mass and distance of the Virgo cluster from a Tolman-Bondi model*', A&A **375**, 770–780.

Glos, V. (2015), '*NFW density profile and shell galaxies*', Bachelor's thesis, Masaryk University.

Hernquist, L. (1990), '*An analytical model for spherical galaxies and bulges*', ApJ **356**, 359–364.

Hernquist, L., Hut, P. & Makino, J. (1993), '*Discreteness Noise versus Force Errors in N-Body Simulations*', ApJ **402**, L85.

Jones, C. & Forman, W. (1984), '*The structure of clusters of galaxies observed with Einstein*', ApJ **276**, 38–55.

Komatsu, E., Smith, K. M., Dunkley, J., Bennett, C. L., Gold, B., Hinshaw, G., Jarosik, N., Larson, D., Nolta, M. R., Page, L., Spergel, D. N., Halpern, M., Hill, R. S., Kogut, A., Limon, M., Meyer, S. S., Odegard, N., Tucker, G. S., Weiland, J. L., Wollack, E. & Wright, E. L. (2011), '*Seven-year Wilkinson Microwave Anisotropy Probe (WMAP) Observations: Cosmological Interpretation*', AJS **192**, 18.

Kravtsov, A. V. & Borgani, S. (2012), '*Formation of Galaxy Clusters*', Annual Review of A&A **50**, 353–409.

Laganá, T. F., Lima Neto, G. B., Andrade-Santos, F. & Cypriano, E. S. (2008), '*Star formation efficiency in galaxy clusters*', A&A **485**, 633–644.

Lee, J., Kim, S. & Rey, S.-C. (2015), '*A New Dynamical Mass Measurement for the VIRGO Cluster Using the Radial Velocity Profile of the Filament Galaxies*', ApJ **807**, 122.

Liddle, A. (2003), *An introduction to modern cosmology; 2nd ed.*, Wiley, Chichester.
URL: *https://cds.cern.ch/record/1010476.*

Markevitch, M. (2006), '*Chandra Observation of the Most Interesting Cluster in the Universe*', ESASP **604**, 723.

Monaghan, J. J. & Lattanzio, J. C. (1985), '*A refined particle method for astrophysical problems*', AJ **149**, 135–143.

Navarro, J. F., Frenk, C. S. & White, S. D. M. (1995), '*The Structure of Cold Dark Matter Halos*', ApJ **462**, 563.

NED (2017), '*NASA/IPAC misc Database: Virgo cluster*'.
URL: *http://ned.ipac.caltech.edu/byname?objname=virgocluster.*

Pandey, V. (2016), '*The comoving volume*'.
URL: *https://www.researchgate.net/post/What_is_comoving_volume.*

Petrovská, Z. (2018), '*Interactions of dark matter and stellar halos in shell galaxies*', Bachelor's thesis, Masaryk University.

Physicsoftheuniverse (2009), '*Graph of how critical density affects the expansion of the universe*'.
URL: *https://www.physicsoftheuniverse.com/topics_bigbang_accelerating.html.*

Riess, A. G., Casertano, S., Yuan, W., Macri, L. M. & Scolnic, D. (2019), '*Large Magellanic Cloud Cepheid Standards Provide a 1% Foundation for the Determination of the Hubble Constant and Stronger Evidence for Physics Beyond LambdaCDM*', arXiv e-prints .

Rogelio B. Andreo (2011), '*Virgo Cluster Deep Widefield*'.
URL: *http://www.deepskycolors.com/archive/2011/03/18/virgo-Cluster-Deep-Widefield.html.*

Ruggiero, R. (2013), '*Clustep*'.
URL: *https://github.com/ruggiero/clustep.*

Ruggiero, R. & Lima Neto, G. B. (2017), '*The fate of the gaseous discs of galaxies that fall into clusters*', MNRAS **468**, 4107–4115.

Ryan, J., Chen, Y. & Ratra, B. (2019), '*Baryon acoustic oscillation, Hubble parameter, and angular size measurement constraints on the Hubble constant, dark energy dynamics, and spatial curvature*', arXiv e-prints .

Sinclair Smith (1936), '*The Mass of the Virgo Cluster*', ApJ **83**, 23.

Springel, V. (2005*a*), '*Gadget-2*'.
URL: *https://wwwmpa.mpa-garching.mpg.de/gadget/.*

Springel, V. (2005*b*), '*The cosmological simulation code GADGET-2*', MNRAS **364**, 1105–1134.

Springel, V. (2005*c*), '*User guide for GADGET-2*'.
    URL: *https://wwwmpa.mpa-garching.mpg.de/gadget/users-guide.pdf.*

Springel, V. & Hernquist, L. (2002), '*Cosmological smoothed particle hydrodynamics simulations: the entropy equation*', MNRAS **333**, 649–664.

Springel, V., Yoshida, N. & White, S. D. M. (2001), '*GADGET: a code for collisionless and gas-dynamical cosmological simulations*', New Astronomy **6**, 79–117.

Tully, R. B. & Fisher, J. R. (1977), '*A new method of determining distances to galaxies*', A&A **54**, 661–673.

Tully, R. B. & Shaya, E. J. (1984), '*Infall of galaxies into the Virgo cluster and some cosmological constraints*', ApJ **281**, 31–55.

Urban, O. (2011), '*On Interactions of Extragalactic Objects*', Master's thesis, Masaryk University.

Urban, O., Werner, N., Simionescu, A., Allen, S. W. & Böhringer, H. (2011), '*X-ray spectroscopy of the Virgo Cluster out to the virial radius*', MNRAS **414**, 2101–2111.

Zejda, M. (2017), '*Kosmologie 2/2*'.
    URL: *http://physics.muni.cz/ zejda/ZA/za2_11_kosmologie2_2017.pdf*